Design and Analysis of a Fault-Tolerant Coplanar Gyro-Free Inertial Measurement Unit

Tsung-Lin Chen

***Abstract*—This paper presents a novel design of a fault-tolerant, coplanar, and gyro-free inertial measurement unit (IMU) that consists of 13 single-axis linear accelerometers and can perform six degree-of-freedom (DOF) measurements for an object in motion. This design uses a combination of redundant accelerometers, an innovative real-time fault-identification technique, together with state-estimation techniques to facilitate robust six DOF measurements, even when some of its accelerometers produce faulty outputs. A design example indicates that the proposed fault-tolerant design and compensation algorithm can detect and correct the biased accelerometer outputs in real time. In this simulation example, the accelerometer measurement noise is assumed to be white and set at 0.1 m/s^2. The minimum detectable dc-offset value is 0.1 m/s^2, which is the same as the standard deviation of the accelerometer measurement noise. The compensated accelerometer outputs were used to construct an "observer-based" gyro-free IMU. The angular-velocity estimation accuracy is 4×10^{-3} rad/s, and the linear-acceleration accuracy is less than 0.24 m/s^2. The IMU output accuracy is not affected by the proposed fault-compensation algorithm. [2006-0225]**

***Index Terms*—Gyro-free inertial measurement unit (IMU), IMU, observability, real-time fault correction, real-time fault identification.**

I. Introduction

INERTIAL measurement units (IMUs) are sensor systems that perform integrated measurement of the six degree-of-freedom (DOF) movement parameters. In this way, one can obtain the position of an object in motion in space, which includes three location coordinates (X, Y, and Z) and three rotation angles (pitch, yaw, and roll). Compared with other sensing techniques that perform six DOF measurements, the IMU has the advantages of mobility and, thus, has been widely used in navigation systems for precise positioning [1], [2].

Generally speaking, there are two ways of constructing six DOF IMUs. The first uses three gyroscopes and three linear accelerometers [1], [3], whereas the second uses linear accelerometers together with signal processing techniques. The second approach is often referred to as a "gyro-free IMU" [4], [5]. The first approach acquires orientation angles of an object in motion by performing a single integral operation on the angular velocities, measured from the gyroscopes. The second approach acquires the orientation angles by performing either a single or double integral operation on the accelerometer outputs, depending on the configuration of the accelerometers. In general, the IMUs that employ gyroscopes have a higher sensing accuracy than the gyro-free IMUs because the former case incorporates gyroscopes with high precision and requires fewer mathematical integral operations.

In previous research, Tan *et al.* [6] proposed a gyro-free IMU configuration, in which six single-axis linear accelerometers were deployed on a cube structure, as shown in Fig. 2. They concluded that the minimum number of single-axis accelerometers needed for stable operation of a gyro-free IMU is six. Instead of using single-axis accelerometers, Ang *et al.* [5] used three dual-axis accelerometers, which not only provided stable IMU operation but also produced three redundant acceleration measurements. They used this redundancy to improve the IMU output accuracy. In many gyro-free IMU designs, the accelerometers were attached to an object at specific locations in a 3-D arrangement to ensure the proper operation of the IMU. As a consequence, it is not only expensive for the assembly but also susceptible to alignment errors that could deteriorate its sensing resolution. Furthermore, to obtain angular velocity, those gyro-free IMU designs either need the initial values of the angular velocity [5], [6] or have difficulties in determining the sign of the angular velocity [7].

Many low-cost micromachined accelerometers employ capacitive sensor mechanisms for acceleration readout. While lateral accelerometers have flourished by adapting this sensing technique, the development of out-of-plane sensing accelerometers has lagged behind due to the severe performance conflict between sensitivity and dynamic range [8] and the large parasitic capacitance to the substrate [9]. In recent years, several techniques have been proposed for developing the out-of-plane sensing accelerometers, including vertical combs [8], differential sensing with multiple metal layers [10], and resonant-type accelerometers [11]. These efforts have made it possible to simultaneously fabricate in-plane and out-of-plane sensing accelerometers on the same substrate while still achieving a comparable performance [10], [11].

Previously, the author proposed a novel observer-based "coplanar" gyro-free IMU design, in which all the employed accelerometers are situated on the same facet of a measurement unit [12]. This approach uses redundant accelerometers together with state-estimation techniques to enable the robust estimation of angular velocity without the need for initial values. Moreover, this approach uses single integral operation to obtain orientation angles, which greatly improves sensing accuracy over other gyro-free IMU designs. However, as with

Manuscript received October 20, 2006; revised August 14, 2007. Subject Editor G. Fedder.

The author is with the Department of Mechanical Engineering, National Chiao Tung University, Hsinchu 300, Taiwan, R.O.C. (e-mail: tsunglin@mail.nctu.edutw).

Color versions of one or more of the figures in this paper are available online at http://ieeexplore.ieee.org.

Digital Object Identifier 10.1109/JMEMS.2007.911372

other IMU designs, this approach does not solve the problem resulting from incorporated sensing elements, producing faulty outputs resulting in erroneous outputs from the IMU.

The purpose of a fault-tolerant sensing system is to maintain system output accuracy when some of the incorporated sensing elements are erroneous. Many fault-tolerant sensing systems are constructed based on "geometric redundancy," which involves having identical sensors deployed at various locations so as to establish algebraic equations for each sensor output. The erroneous sensor unit can be identified by these equations and excluded from the sensor array [13]–[15]. Many research reports address geometric-redundancy designs for gyroscopes, but only a few cover the linear accelerometers. In those few reports, fault-identification tests were performed only when the object is either under linear motion or at rest [16].

For fault-tolerant designs, the conventional approach to "fault identification" is through the use of "voting equations" [13], [14]. If the outputs from the incorporated sensing devices (systems) are contaminated by noise, with the conventional approach, one has to set up threshold values and an observation period along with the voting equations. When the outputs from the voting equations exceed the threshold value at the end of the observation period, faulty-sensor recognition is declared. The need for an observation period means that the conventional approach cannot be done in real time. As a consequence, a real-time "fault-correction" method is not attainable.

This paper proposes a fault-tolerant design for the observer-based coplanar gyro-free IMU. This design uses more redundant coplanar accelerometers to realize a novel fault-compensation algorithm. As such, the faulty sensors in the IMU can be detected and compensated in real time, and the corrected devices can be retained in the IMU system to further increase system output accuracy. Moreover, all incorporated accelerometers can be simultaneously fabricated *in situ* onto a substrate using accelerometer-fabrication processes. These unique features facilitate the concept of a MEMS system-on-chip gyro-free IMU design that greatly reduces fabrication cost and alignment errors.

This paper is organized as follows. The basics of the observer-based gyro-free IMU are introduced in Section II. The design procedures of the observer-based coplanar gyro-free IMU are discussed in Section III. In Section IV, a design of the fault-tolerant coplanar gyro-free IMU system is first presented, followed by the introduction of the proposed real-time fault-compensation algorithm. The signal processing associated with the IMU design is shown in Section V. This includes the stability analysis of the algorithm and some simulation results. The discussion of this design is shown in Section VI. Finally, Section VII concludes this paper.

II. Observer-Based Gyroscope-Free IMU

A. Gyroscope-Free IMU Theory

Fig. 1 shows the relation between the earth-centered inertial frame $\{e\}$ and the body frame $\{b\}$. $\vec{R}_o$ is a position vector from the earth center to the center of the body frame. $\vec{R}_j$ is a position vector from the earth center to the location j, and $\vec{r_j}$ is a position vector from the center of the body frame to the location j. $\vec{w}$ is the rotation rate of the body frame. By using the coordinate transformation, the acceleration at location j can be written as follows:

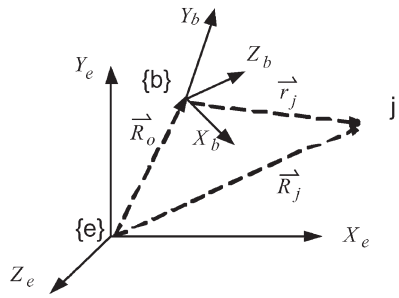

Fig. 1. Schematic of inertial frame versus body frame.

$$\ddot{\vec{R}}_j = \ddot{\vec{R}}_o + \dot{\vec{w}} \times \vec{r_j} + \vec{w} \times (\vec{w} \times \vec{r_j}) + 2\vec{w} \times \dot{\vec{r}}_j + \ddot{\vec{r}}_j. \quad (1)$$

In the case that the body frame is rotated with the object in motion, the $\vec{r_j}$ vector represented in the body frame ${}^b r_j$ is constant. Therefore, (1) can be simplified as follows:

$$\begin{aligned} {}^e\ddot{R}_j &= {}^e\ddot{R}_o + C_b^e\, {}^b\dot{w} \times {}^b r_j + C_b^e\, {}^b w \times ({}^b w \times {}^r r_j) \\ {}^e\ddot{R}_j &= {}^e F_j \end{aligned} \quad (2)$$

where ${}^e F_j$ is the specific force [6] applied at the location j and represented in the inertial frame, and C_b^e is the conversion matrix for transforming a vector represented in the body frame into a vector represented in the inertial frame. By assuming that a single-axis accelerometer is rigidly mounted on the object at the location j with a sensing direction of $\vec{\eta_j}$, the accelerometer output A_j can then be written as

$$\begin{aligned} A_j &= \ddot{\vec{R}}_j \cdot \vec{\eta_j} = {}^b\ddot{R}_j{}^{\mathrm{T}}\, {}^b\eta_j \\ &= \left[\left({}^b r_j \times {}^b\eta_j\right)^{\mathrm{T}}\ {}^b\eta_j \right] \begin{bmatrix} {}^b\dot{w} \\ {}^b F_o \end{bmatrix} + {}^b\eta_j{}^{\mathrm{T}}\ \left({}^b w \times \left({}^b w \times {}^b r_j\right)\right). \end{aligned} \quad (3)$$

By supposing that there are m accelerometers distributed on the object, the accelerometer measurements can be arranged in the following vector form:

$$\begin{bmatrix} A_1 \\ \vdots \\ A_m \end{bmatrix} = J \begin{bmatrix} {}^b\dot{w} \\ {}^b F_o \end{bmatrix} + \begin{bmatrix} {}^b\eta_1{}^{\mathrm{T}}\ \left({}^b w \times \left({}^b w \times {}^b r_1\right)\right) \\ \vdots \\ {}^b\eta_m{}^{\mathrm{T}}\ \left({}^b w \times \left({}^b w \times {}^b r_m\right)\right) \end{bmatrix}$$

$$J = \begin{bmatrix} \left({}^b r_1 \times {}^b\eta_1\right)^{\mathrm{T}} & {}^b\eta_1 \\ \vdots & \\ \left({}^b r_m \times {}^b\eta_m\right)^{\mathrm{T}} & {}^b\eta_m \end{bmatrix}. \quad (4)$$

If the matrix $J^{\mathrm{T}}J$ is invertible, the relation between the dynamics of object in motion and the measurements from accelerometers located at various locations can be shown as follows:

$$\begin{bmatrix} {}^b\dot{w} \\ {}^bF_o \end{bmatrix} = (J^{\mathrm{T}}J)^{-1}J^{\mathrm{T}} \times \left(\begin{bmatrix} A_1 \\ \vdots \\ A_m \end{bmatrix} - \begin{bmatrix} {}^b\eta_1{}^{\mathrm{T}} \left({}^bw \times \left({}^bw \times {}^br_1\right)\right) \\ \vdots \\ {}^b\eta_m{}^{\mathrm{T}} \left({}^bw \times \left({}^bw \times {}^br_m\right)\right) \end{bmatrix} \right). \tag{5}$$

By excerpting from (5), one can obtain a set of nonlinear differential equations for the angular velocity

$$\left[{}^b\dot{w}\right]_{3\times 1} = (J^{\mathrm{T}}J)^{-1}J^{\mathrm{T}}(1:3,:)\ldots \times \left(\begin{bmatrix} A_1 \\ \vdots \\ A_m \end{bmatrix} - \begin{bmatrix} {}^b\eta_1{}^{\mathrm{T}} \left({}^bw \times \left({}^bw \times {}^br_1\right)\right) \\ \vdots \\ {}^b\eta_m{}^{\mathrm{T}} \left({}^bw \times \left({}^bw \times {}^br_m\right)\right) \end{bmatrix} \right) \tag{6}$$

which is referred to as the "governing equation" of the gyro-free IMU system in this paper.

Based on the governing equation, for $(J^{\mathrm{T}}J)^{-1}$ to exist, the minimum number of accelerometers required is six. These six single-axis accelerometers, which are employed for constructing the governing equation, are referred to as the "system accelerometers" in this paper.

After acquiring the governing equation, the operation of a gyro-free IMU then becomes an "observer" problem, which means that the angular velocity is obtained through associated governing equations. Therefore, provided with the initial values of angular velocities, one can use (6) to calculate the angular velocities along a trajectory. Once the values of the angular velocities are obtained, the linear accelerations can be calculated from (5).

B. Observer-Based Gyro-Free IMU

From a system observability viewpoint [17], it is more robust to have a "closed-loop observer" than an "open-loop observer." Moreover, a closed-loop observer does not need initial conditions for state estimation. Therefore, it is beneficial to employ redundant accelerometers to create "outputs" for the gyro-free IMU system so as to implement a robust closed-loop observer [12]. These accelerometers are referred to as "observer accelerometers" in this paper. Since they are accelerometers deployed in the IMU, these observer accelerometers can be described by (3), and their outputs can be arranged in a way that associates them with the outputs from the system accelerometers. As a result, the observer accelerometer output, A_{oj} in (7), consists of measurements from the system accelerometers and the angular velocities only, and thus, they can be treated as the system outputs for a gyro-free IMU system

$$\begin{bmatrix} A_{o1} \\ \vdots \\ A_{oj} \\ \vdots \\ A_{om} \end{bmatrix} = \begin{bmatrix} \left({}^br_{o1} \times {}^b\eta_{o1}\right)^{\mathrm{T}} & {}^b\eta_{o1} \\ \vdots & \\ \left({}^br_{oj} \times {}^b\eta_{oj}\right)^{\mathrm{T}} & {}^b\eta_{oj} \\ \vdots & \\ \left({}^br_{om} \times {}^b\eta_{om}\right)^{\mathrm{T}} & {}^b\eta_{om} \end{bmatrix} (J^{\mathrm{T}}J)^{-1}J^{\mathrm{T}}\ldots \times \left(\begin{bmatrix} A_1 \\ \vdots \\ A_m \end{bmatrix} - \begin{bmatrix} {}^b\eta_1{}^{\mathrm{T}} \left({}^bw \times \left({}^bw \times {}^br_1\right)\right) \\ \vdots \\ {}^b\eta_m{}^{\mathrm{T}} \left({}^bw \times \left({}^bw \times {}^br_m\right)\right) \end{bmatrix} \right) + \begin{bmatrix} {}^b\eta_{o1}{}^{\mathrm{T}} \left({}^bw \times \left({}^bw \times {}^br_{o1}\right)\right) \\ \vdots \\ {}^b\eta_{oj}{}^{\mathrm{T}} \left({}^bw \times \left({}^bw \times {}^br_{oj}\right)\right) \\ \vdots \\ {}^b\eta_{om}{}^{\mathrm{T}} \left({}^bw \times \left({}^bw \times {}^br_{om}\right)\right) \end{bmatrix} \tag{7}$$

where ${}^br_{oj}$ and ${}^b\eta_{oj}$ represent the respective location and the sensing direction of an observer accelerometer.

In a dynamic system, the rank of the observability matrix and its associated singular values are indicators of a feasible observer design [18]. The observability matrix of a nonlinear system can be obtained as follows:

$$W_o = \bigtriangledown[z\ \dot{z}\ \ldots]^{\mathrm{T}}, \quad z = [A_{o1}\ldots A_{oj}\ldots A_{om}]. \tag{8}$$

Although, in theory, one should design the accelerometer configuration (number of incorporated accelerometers, locations, sensing directions, and so forth) based on the system observability matrix, it is extremely difficult to do so. This is not only because the analytical solution of the observability matrix is complicated but also because the observability of a nonlinear system depends on the angular velocities to be measured. Furthermore, when the angular velocity to be measured is constant, the derivatives of the IMU outputs are zero, and the row vectors in the observability matrix are reduced. In turn, the rank of the observability matrix is reduced. For these reasons, an IMU system needs at least three outputs to ensure that the rank of its observability matrix is three.

III. Observer-Based Coplanar Gyro-Free IMU

A. Design of Coplanar System Accelerometers

The way to construct governing equations for a planar-type gyro-free IMU, while minimizing the number of accelerometers, is to employ a set of three accelerometers that measure the acceleration along the direction parallel to the plane surface of the measurement unit (in-plane sensing) and another set of three accelerometers that measure the acceleration along the direction perpendicular to the plane surface of the measurement unit (out-of-plane sensing) [12]. Fig. 2 compares a cube-type gyro-free IMU with the proposed coplanar gyro-free IMU design.

For an in-plane sensing accelerometer located at $[r\cos\alpha_j\, r\sin\alpha_j 0]^{\mathrm{T}}$ with sensing direction $[\cos\beta_j \sin\beta_j 0]^{\mathrm{T}}$,

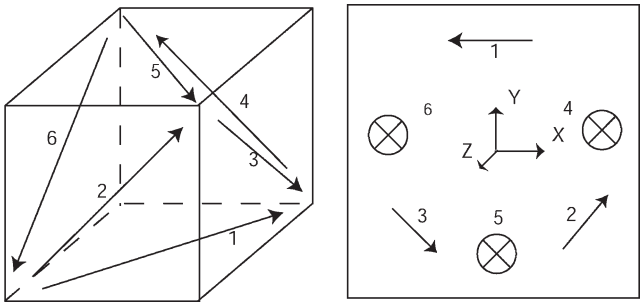

Fig. 2. Cube-type gyro-free IMU versus coplanar gyro-free IMU. The arrow denotes the sensing direction of each accelerometer. ($\longrightarrow$) denotes the in-plane sensing accelerometers; ($\otimes$) denotes the out-of-plane sensing accelerometers.

the accelerometer output, which is derived from (3), can be simplified to

$$A_{i-p,j} = \begin{bmatrix} r\sin(\beta_j - \alpha_j) \\ \cos\beta_j \\ \sin\beta_j \\ -r\sin\alpha_j \sin\beta_j \\ -r\cos\alpha_j \cos\beta_j \\ r\sin(\alpha_j + \beta_j) \end{bmatrix}^{\mathrm{T}} \begin{bmatrix} \dot{w}_3 \\ F_{o1} \\ F_{o2} \\ w_1^2 + w_3^2 \\ w_2^2 + w_3^2 \\ w_1 w_2 \end{bmatrix} = H_{i-p} \begin{bmatrix} \dot{w}_3 \\ F_{o1} \\ F_{o2} \\ w_1^2 + w_3^2 \\ w_2^2 + w_3^2 \\ w_1 w_2 \end{bmatrix}. \quad (9)$$

Similarly, for an out-of-plane sensing accelerometer located at $[r\cos\alpha_j r\sin\alpha_j 0]^{\mathrm{T}}$ with sensing direction $[0\,0\,1]^{\mathrm{T}}$, the accelerometer output can be simplified to

$$A_{o-p,j} = \begin{bmatrix} r\sin\alpha_j \\ r\cos\alpha_j \\ 1 \\ r\cos\alpha_j \\ r\sin\alpha_j \end{bmatrix}^{\mathrm{T}} \begin{bmatrix} \dot{w}_1 \\ \dot{w}_2 \\ F_{o3} \\ w_1 w_3 \\ w_2 w_3 \end{bmatrix} = H_{o-p} \begin{bmatrix} \dot{w}_1 \\ \dot{w}_2 \\ F_{o3} \\ w_1 w_3 \\ w_2 w_3 \end{bmatrix}. \quad (10)$$

B. Design of Coplanar Observer Accelerometers

Since the observer accelerometers in a coplanar configuration must be in-plane and/or out-of-plane sensing accelerometers, the design of coplanar observer accelerometers can be separated into that for the in-plane and out-of-plane sensing accelerometers.

From (9), the outputs of multiple in-plane sensing accelerometers can be organized as follows:

$$\begin{bmatrix} \vdots \\ A_j \\ \vdots \end{bmatrix} - r \begin{bmatrix} & -\sin(\alpha_j)\sin(\beta_j) & \\ \vdots & -\cos(\alpha_j)\cos(\beta_j) & \vdots \\ & \sin(\alpha_j + \beta_j) & \end{bmatrix}^{\mathrm{T}} \begin{bmatrix} w_1^2 + w_3^2 \\ w_2^2 + w_3^2 \\ w_1 w_2 \end{bmatrix} = \begin{bmatrix} & \vdots & \\ r\sin(\beta_j - \alpha_j) & \cos\beta_j & \sin\beta_j \\ & \vdots & \end{bmatrix} \begin{bmatrix} \dot{w}_z \\ F_{o1} \\ F_{o2} \end{bmatrix}. \quad (11)$$

With multiple in-plane sensing accelerometers, the H_{i-p} term in (9) can provide at most six independent column vectors. Therefore, there exists a matrix U (see the Appendix) such that

$$U \begin{bmatrix} & -\sin(\alpha_j)\sin(\beta_j) & \\ \vdots & -\cos(\alpha_j)\cos(\beta_j) & \vdots \\ & \sin(\alpha_j + \beta_j) & \end{bmatrix}^{\mathrm{T}} \neq 0$$

$$U \begin{bmatrix} & \vdots & \\ r\sin(\beta_j - \alpha_j) & \cos(\beta_j) & \sin(\beta_j) \\ & \vdots & \end{bmatrix} = 0. \quad (12)$$

Combining (11) and (12) results in (13), which describes the relations between the accelerometer outputs and the angular velocities

$$U \begin{bmatrix} & -\sin(\alpha_j)\sin(\beta_j) & \\ \vdots & -\cos(\alpha_j)\cos(\beta_j) & \vdots \\ & \sin(\alpha_j + \beta_j) & \end{bmatrix}^{\mathrm{T}} \begin{bmatrix} w_1^2 + w_3^2 \\ w_2^2 + w_3^2 \\ w_1 w_2 \end{bmatrix} = U \begin{bmatrix} \vdots \\ A_j \\ \vdots \end{bmatrix}. \quad (13)$$

Thus, (13) is a special case of (7) with the in-plane sensing accelerometers only and can be treated as the system outputs of a coplanar gyro-free IMU. Furthermore, based on the Appendix, the maximum rank of the matrix U in (14) is three, which can be achieved by a minimum of six in-plane sensing accelerometers. Therefore, by using three in-plane sensing accelerometers as the observer accelerometers, in addition to three system accelerometers, one can obtain three independent output equations for the coplanar IMU system

$$\underset{\alpha_j,\beta_j}{\mathrm{Max}} \quad \mathrm{rank}\left(U \begin{bmatrix} & -\sin(\alpha_j)\sin(\beta_j) & \\ \vdots & -\cos(\alpha_j)\cos(\beta_j) & \vdots \\ & \sin(\alpha_j + \beta_j) & \end{bmatrix}^{\mathrm{T}} \right) = 3. \quad (14)$$

By following the same procedure, it can be shown that the out-of-plane sensing accelerometers cannot be utilized as the observer accelerometers.

IV. Fault-Tolerant Design for Coplanar Gyro-Free IMU Systems

A. Fault-Tolerant Theory

Most fault-tolerant designs start with the following equation, which is well-suited for the "geometric-redundancy" design:

$$m = H\,X + e \quad (15)$$

where m is a vector of the sensor measurements, X is the state vector of the system, and e is the noise that contaminates the

measurements. Let H^* be the transpose conjugate of H and V be the null space of H^*, then

$$V^* H = 0.$$

The "parity equations," which are widely applied to the fault-tolerant systems, are defined as follows:

$$\text{Parity Equations} \equiv V^* m. \tag{16}$$

Therefore, if all the sensors function properly, the outputs of the parity equations are expected to be zero mean. As shown in previous research [13]–[15], a system with n states needs $n+1$ sensors to form one parity equation, $n+2$ sensors to form two parity equations, and so forth. Furthermore, by assuming that only one faulty sensor exists in a sensor array, the system needs at least two parity equations to locate it.

These two parity equations are often converted into $n+2$ equations, each involving $n+1$ sensor outputs. That is to say, one can form a $(n+2) \times (n+2)$ matrix with its diagonal terms equal to zero but nonzero elsewhere. The newly formed equations are referred to as the "voting equations" with an associated "voting matrix" to distinguish them from the "parity equations."

$$\begin{aligned}\text{Voting Equations} &\equiv C_{\text{voting}} \cdot \begin{bmatrix} m_1 \\ \vdots \\ m_{n+2} \end{bmatrix} \\ C_{\text{voting}} &= \begin{bmatrix} 0 & c_{12} & \cdots & c_{1,n+2} \\ c_{21} & 0 & \cdots & c_{2,n+2} \\ \vdots & & & \vdots \\ c_{n+2,1} & \cdots & c_{n+2,n+1} & 0 \end{bmatrix} \\ &= \begin{bmatrix} C_{\text{vot } 1} \\ C_{\text{vot } 2} \\ \vdots \\ C_{\text{vot } n+2} \end{bmatrix}\end{aligned} \tag{17}$$

where $C_{\text{vot } 1} \cdots C_{\text{vot } n+2}$ are the row vectors of C_{voting} and are adopted here for clarity of presentation. A faulty sensor is easier to identify from the voting equations than from the parity equations. For example, if the output of the first voting equation is zero but the rest are nonzeros, one can determine that measurement m_1 is faulty. Furthermore, since the voting matrix is derived from the two parity equations, its rank is two.

B. Fault-Tolerant Design for Gyro-Free IMU

As shown in (4), the output of a linear accelerometer that is attached to a moving object is a function of linear acceleration, angular acceleration, and angular velocity. Furthermore, the very last term in (4) is comprised of second-order terms of the three angular velocities and, thus, can be of nine different combinations. Therefore, to realize the geometric-redundancy design for these linear accelerometers, one needs to have 15 system states in (15): three from the linear accelerations, three from the angular acceleration, and nine from the angular velocity of the second order. Consequently, 17 accelerometers are required for a fault-tolerant gyro-free IMU design. Only one faulty accelerometer is allowed, which can be identified by checking on the 17 voting equations.

C. Fault-Tolerant Design for Coplanar Gyro-Free IMU

Fault-tolerant design of a gyro-free IMU can be greatly simplified if it is in the proposed coplanar configuration. As shown in (9) and (10), the outputs of the in-plane and out-of-plane sensing accelerometers possess totally different system states. Therefore, the design task of using a minimum number of accelerometers to construct a fault-tolerant coplanar gyro-free IMU system can be separated into that for the in-plane and out-of-plane sensing accelerometers. With proper choice of locations and sensing directions for certain accelerometers in (9), H_{i-p} can provide six independent column vectors. Therefore, the associated fault-tolerant design needs eight in-plane sensing accelerometers, allowing only one to go awry to identify the faulty one. Similarly, with (10), H_{o-p} can provide three independent column vectors. Therefore, the associated fault-tolerant design needs five out-of-plane sensing accelerometers, allowing only one to go awry to identify the faulty one.

As compared with the noncoplanar configuration, the coplanar configuration can identify more faulty sensors with few sensors.

D. Novel Real-Time Fault-Compensation Algorithm

As discussed before, the conventional fault-identification techniques cannot be applied in real time when the measurements are contaminated by noise. Here, a novel real-time fault-compensation method is proposed for the case when outputs from incorporated sensors are contaminated by noise and experience dc offset. This approach can be divided into two parts: real-time fault identification and real-time fault correction.

In the fault-identification part, the dc offset, d_j in (18), is first separated from the sensor output and modeled as system states

$$A_{\text{dc}\,j} = A_j + d_j, \quad j = 1, \ldots, n+2 \tag{18}$$

where $A_{\text{dc}\,j}$ is the sensor output with dc offset and white noise, and A_j is the sensor output without dc offset but contaminated by white noise. When these dc offsets are treated as system states, their governing equations, which are derived for discrete-time applications, can be written as follows:

$$d_j(k+1) = d_j(k), \quad j = 1, \ldots, n+2. \tag{19}$$

Since the aforementioned system is static, from a system observability viewpoint, it needs $n+2$ output equations to observe $n+2$ states. The two parity equations, which were originally used to describe the relations between outputs from

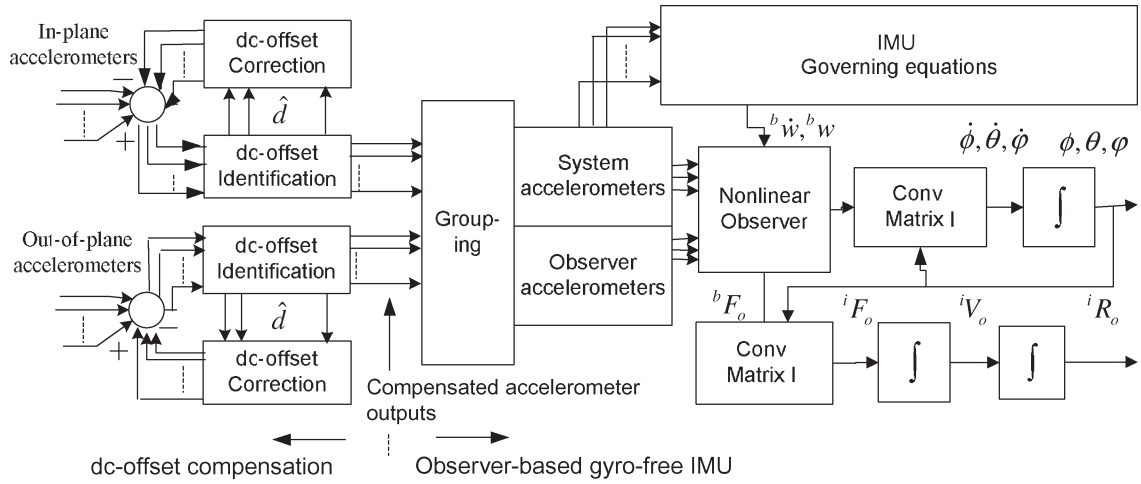

Fig. 3. Block diagram of the proposed fault-tolerant coplanar gyro-free IMU.

the $n+2$ sensors, can be processed to obtain two output equations for the dc-offset state estimation. These two parity equations can be chosen by arbitrary taking two row vectors from a "voting matrix," such as Z_{p} shown in

$$\begin{aligned} Z_{\mathrm{p}} : \begin{bmatrix} C_{\mathrm{vot}\ 1} \\ C_{\mathrm{vot}\ 2} \end{bmatrix} \begin{bmatrix} d_1 \\ \vdots \\ d_{n+2} \end{bmatrix} \\ = \begin{bmatrix} C_{\mathrm{vot}\ 1} \\ C_{\mathrm{vot}\ 2} \end{bmatrix} \begin{bmatrix} A_{\mathrm{dc}\ 1} - A_1 \\ \vdots \\ A_{\mathrm{dc}\ n+2} - A_{n+2} \end{bmatrix} \\ = \begin{bmatrix} C_{\mathrm{vot}\ 1} \\ C_{\mathrm{vot}\ 2} \end{bmatrix} \begin{bmatrix} A_{\mathrm{dc}\ 1} \\ \vdots \\ A_{\mathrm{dc}\ n+2} \end{bmatrix} \\ Z_{\mathrm{aux}} : C_{\mathrm{voting}} \begin{bmatrix} d_1 \\ \vdots \\ d_{n+2} \end{bmatrix} e_i d_i \\ = C_{\mathrm{voting}} \begin{bmatrix} A_{\mathrm{dc}\ 1} \\ \vdots \\ A_{\mathrm{dc}\ n+2} \end{bmatrix} e_i d_i + \begin{bmatrix} v_1 \\ \vdots \\ v_{n+2} \end{bmatrix}, \\ i = 1, 2, \ldots, n+2. \end{aligned} \tag{20}$$

The remaining output equations assume that only one faulty sensor exists in a sensor array; this leads to the Z_{aux} equations shown in (20). In that equation, e_i is the unitary vector, and v_i is the fictitious noise required for the extended Kalman filter (EKF). The formulation of these Z_{aux} equations is the key to the success of the proposed real-time fault-compensation method.

Once the dc offset of each sensor is identified in real time, the accompanying fault-correction measure can be obtained from various control methods. In this paper, the real-time fault correction is formulated as state feedback for linear systems. The compensated accelerometer outputs $A_{\mathrm{comp}\ j}$, which are derived for the discrete-time applications, can be obtained as follows:

$$\begin{aligned} \hat{d}_j(k+1) &= \hat{d}_j(k) - \lambda \hat{d}(k) \\ A_{\mathrm{comp}\ j}(k+1) &= A_{\mathrm{dc}\ j}(k+1) - \lambda \sum_{i=0}^{k} \hat{d}_j(i). \end{aligned} \tag{21}$$

The accelerometer measurements are compensated by the estimation of dc offset in real time. This approach is very similar to the conventional linear-quadratic-Gaussian (LQG) methods [19]; the only difference is that the Kalman filter is replaced by the EKF.

V. Data Processing

A. Block Diagram

Fig. 3 shows a schematic of the proposed fault-tolerant coplanar gyro-free IMU. The processing of accelerometer outputs can be divided into two phases. In the first phase, the outputs of the in-plane and out-of-plane sensing accelerometers are separately processed with the real-time dc-offset compensation algorithm. The compensated accelerometer outputs are regrouped into the system and observer accelerometers for the subsequent observer-based gyro-free IMU operation.

The feedback loop shown in the proposed scheme takes place at the dc-offset compensation. Therefore, the stability analysis for the overall system can be proceeded for the dc-offset compensation and the nonlinear state estimation, independently.

B. Stability Analysis for DC-Offset Compensation

The stability of the first part is essentially a task of stabilizing a nonlinear system using estimated state values. According to Vidyasagar [20], the separation property [17], which is often discussed for the linear systems, can be applied to the nonlinear systems to guarantee their local asymptotical stability. Therefore, the stability analysis here can be further divided into two tasks: one for a stabilizing controller design and the

other for a stable observer design. From (21), it can be quickly shown that if the feedback gain λ is chosen between zero and two, the corresponding eigenvalues of the feedback system are between -1 and 1, and thus, it is a stabilizing controller. For a stable observer design, one needs to prove that the system, as shown in (19) and (20), is an observable system, and the employed observer algorithm can achieve a stabilizing observer design.

Since the dc-offset system is static, the observability matrix is solely composed of the Jacobian matrix of output equations and can be processed as follows:

$$\begin{aligned}&\operatorname{rank}\left(\nabla[Z_{\mathrm{p}} \quad Z_{\mathrm{aux}}]^{\mathrm{T}}\right)\\ &= \operatorname{rank}\begin{bmatrix} C_{\mathrm{vot}\ 1} \\ C_{\mathrm{vot}\ 2} \\ d_1 C_{\mathrm{vot}\ 1} + [C_{\mathrm{vot}\ 1} d\ 0\ 0\ \cdots\ 0] \\ \vdots \\ d_{n+2} C_{\mathrm{vot}\ n+2} + [0\ \cdots\ 0\ 0\ C_{\mathrm{vot}\ n+2} d] \end{bmatrix}\\ &= \operatorname{rank}\left[\begin{bmatrix} C_{\mathrm{vot}\ 1} \\ C_{\mathrm{vot}\ 2} \end{bmatrix} \begin{bmatrix} C_{\mathrm{vot}\ 1} d & 0 & 0 & \cdots & 0 \\ \vdots & & & & \\ 0 & \cdots & 0 & 0 & C_{\mathrm{vot}\ n+2} \end{bmatrix}\right]. \end{aligned} \tag{22}$$

The rank of the aforementioned matrix can be determined by examining the matrix $[C_{\mathrm{vot}\ 1} C_{\mathrm{vot}\ 2}]^{\mathrm{T}}$ from (22) in the upper half and the diagonal matrix in the lower half. The diagonal matrix is exactly the outcome of the voting equations. Therefore, exactly one element along the diagonal terms is zero. In turn, the diagonal matrix provides $n+1$ independent row vectors for the overall matrix. Furthermore, since $C_{\mathrm{vot}\ 1}$ and $C_{\mathrm{vot}\ 2}$ are two row vectors in a voting matrix, zero should not appear in the same column of these two vectors, and thus, it provides one more independent row vector for the overall matrix. As a consequence, the rank of the observability matrix is $n+2$ globally. In other words, the system is globally observable.

The question that remains is whether the EKF is a stabilizing observer algorithm for this dc-offset estimation. It is known that the EKF is effective in noise reduction but its state convergence is not guaranteed [21]. In that case, one can use the iterative Kalman filter (IKF) to achieve both the state convergence and the noise reduction.

C. Stability Analysis for the Angular-Velocity Estimation

Stability analysis of the second part aims to show whether the proposed observer-based gyro-free IMU design can successfully estimate the angular velocities. Similar to the discussion before, this problem can be approached by examining if the proposed coplanar configuration constitutes an observable system and if the associated observer algorithm is a feasible algorithm to ensure state convergence.

Based on Section II-B, the observability check for the proposed IMU design can proceed by simply checking the Jacobian of the output equations. Since the output equations of the coplanar gyro-free IMU are composed of the in-plane sensing accelerometers only, the observability matrix can be obtained by taking the Jacobian of (13).

$$\nabla \begin{bmatrix} \vdots \\ z \\ \vdots \end{bmatrix} = U \begin{bmatrix} & -\sin(\alpha_j)\sin(\beta_j) & \\ \vdots & -\cos(\alpha_j)\cos(\beta_j) & \vdots \\ & \sin(\alpha_j+\beta_j) & \end{bmatrix}^{\mathrm{T}} \cdot \begin{bmatrix} 2w_1 & 0 & 2w_3 \\ 0 & 2w_2 & 2w_3 \\ w_2 & w_1 & 0 \end{bmatrix}. \tag{23}$$

As discussed in Section III-B, the design of the observer accelerometers is to ensure a rank of three for the product of the first two terms on the right-hand side of (23); this leads to the following conclusions:

$$\begin{aligned}&\operatorname{rank}\left(\begin{bmatrix} 2w_1 & 0 & 2w_3 \\ 0 & 2w_2 & 2w_3 \\ w_2 & w_1 & 0 \end{bmatrix}\right) = 3\\ &\Rightarrow w_3(w_1^2 - w_2^2) \neq 0. \end{aligned} \tag{24}$$

Therefore, as long as $w_3 \neq 0$ and $w_1 \neq \pm w_2$ along the entire trajectory, it is an observable system. Thus, three angular velocities are observable with a proper algorithm. In this case, the IKF is employed as the collaborated observer algorithm to ensure both the state convergence and the noise reduction.

D. Simulation Case

This section presents simulation results for an example design incorporating 13 single-axis accelerometers being distributed on the periphery of a circular disk to form a coplanar gyro-free IMU. Since the size of the disk affects only the sensing resolution of the IMU, which has already been discussed in the previous paper [12], without losing generality and to increase the visibility of the plots, the radius of the disk was set to one. The location and the sensing direction of each accelerometer are listed in Table I. The accelerometers that are marked xL1, xL2, xL4, xL5, xL7, xL8, xL10, and xL12 are the in-plane sensing accelerometers, whereas the ones marked xL3, xL6, xL9, xL11, and xL13 are the out-of-plane sensing accelerometers. xL1, xL5, xL8, xL3, xL6, and xL9 were selected as the system accelerometers, whereas xL2, xL7, and xL4 were selected as the observer accelerometers. The trajectories to be measured are the following: three constant Euler angle rotation rates of 36, 72, and 54 deg/s, respectively, and three linear accelerations of 1, 2, and 5 m/s^2, respectively, in the inertial frame. To demonstrate the proposed fault-tolerant design, one of the in-plane sensing accelerometers, xL1 in this case, was arbitrarily chosen to be dc-biased at 4 m/s^2, and one of the out-of-plane sensing accelerometers, xL6 in this case, was chosen to be dc-biased at 6 m/s^2. Without loss of generality, the noise associated with each accelerometer measurement was assumed to be white with the same standard deviation of 0.1 m/s^2; this leads to a signal-to-noise ratio (SNR) of four for the angular-velocity estimation.

TABLE I
COPLANAR CONFIGURATION OF 13 SINGLE-AXIS ACCELEROMETERS

Accel. number	Location ${}^b r_j(x, y, z)$	Sensing direction ${}^b \eta_j(x, y, z)$
xL1	$r[cos(2\pi/14) \quad sin(2\pi/14) \quad 0]$	$[cos(9\pi/14) \quad sin(9\pi/14) \quad 0]$
xL2	$r[cos(4\pi/14) \quad sin(4\pi/14) \quad 0]$	$[cos(13\pi/21) \quad sin(13\pi/21) \quad 0]$
xL3	$r[cos(6\pi/14) \quad sin(6\pi/14) \quad 0]$	$[0 \quad 0 \quad 1]$
xL4	$r[cos(8\pi/13) \quad sin(8\pi/13) \quad 0]$	$[cos(45\pi/52) \quad sin(45\pi/52) \quad 0]$
xL5	$r[cos(10\pi/14) \quad sin(10\pi/14) \quad 0]$	$[cos(26\pi/33) \quad sin(26\pi/33) \quad 0]$
xL6	$r[cos(12\pi/14) \quad sin(12\pi/14) \quad 0]$	$[0 \quad 0 \quad 1]$
xL7	$r[cos(14\pi/14) \quad sin(14\pi/14) \quad 0]$	$[cos(41\pi/26) \quad sin(41\pi/26) \quad 0]$
xL8	$r[cos(16\pi/14) \quad sin(16\pi/14) \quad 0]$	$[cos(16\pi/13) \quad sin(16\pi/13) \quad 0]$
xL9	$r[cos(18\pi/14) \quad sin(18\pi/14) \quad 0]$	$[0 \quad 0 \quad 1]$
xL10	$r[cos(20\pi/14) \quad sin(20\pi/14) \quad 0]$	$[cos(93\pi/52) \quad sin(93\pi/52) \quad 0]$
xL11	$r[cos(22\pi/14) \quad sin(22\pi/14) \quad 0]$	$[0 \quad 0 \quad 1]$
xL12	$r[cos(28\pi/14) \quad sin(28\pi/14) \quad 0]$	$[cos(21\pi/52) \quad sin(21\pi/52) \quad 0]$
xL13	$r[cos(26\pi/14) \quad sin(26\pi/14) \quad 0]$	$[0 \quad 0 \quad 1]$

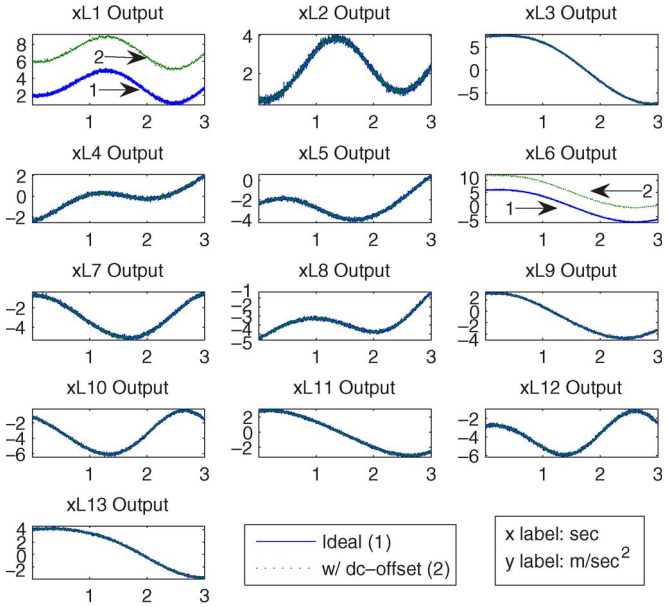

Fig. 4. Accelerometer outputs along a trajectory. The outputs of accelerometers xL1 and xL6 are dc-biased.

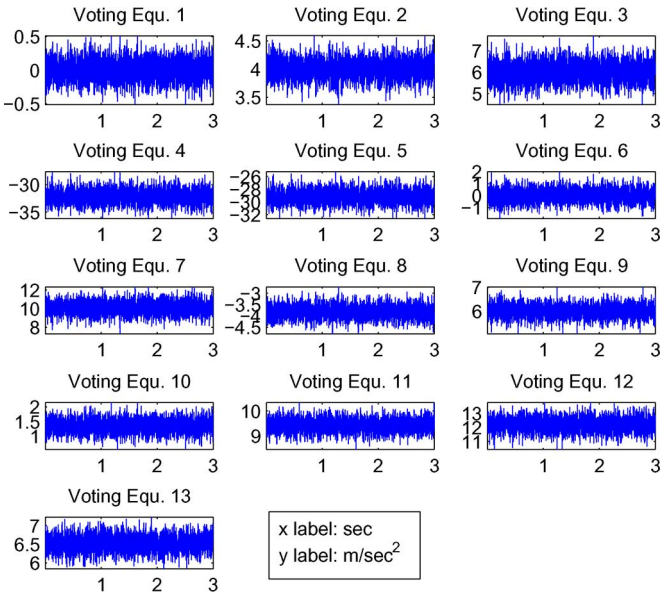

Fig. 5. Outputs of the voting equations along a trajectory. The first and sixth plots are of zero means, but the rest are all of nonzero means.

The 13 accelerometer measurements along a trajectory are shown in Fig. 4. As evident from the plots, all accelerometer measurements are contaminated by noise, and the outputs of xL1 and xL6 are dc-biased.

Fig. 5 shows the noise-contaminated outputs of the voting equations for the accelerometer array. Only the first and sixth plots have zero means, whereas the remainder have nonzero means. The first and sixth plots are the cases where the outputs of xL1 and xL6 are absent from their respective voting equations. Thus, by observing the outcomes of the voting equations over a period of time, one can determine that the outputs of xL1 and xL6 are dc-biased.

Fig. 6 shows the dc-offset estimation for the accelerometer outputs. As shown in the plot, the proposed estimation algorithm can correctly estimate the dc-bias value for each accelerometer in real time. The standard deviations of the estimated values all decrease to 0.01 m/s^2 after 0.6 s, owing to the EKF, which is one order less than the standard deviation of the accelerometer measurement noise.

Fig. 7 shows the accelerometer outputs after having been processed with the dc-offset compensation algorithm. The feedback gain in the compensation algorithm is 0.005. Based on the simulation results, all accelerometer outputs converge to their correct values after approximately 0.6 s, and the associated standard deviations are between 0.103 and 0.097 m/s^2 after 1 s.

Fig. 8 shows the estimation of the angular velocities using the compensated accelerometer outputs. Simulation results indicate that the estimated values of the angular velocity converge to their correct values roughly at 1 s. Furthermore, owing to the IKF algorithm, the standard deviations of the estimated values are 4×10^{-3} rad/s.

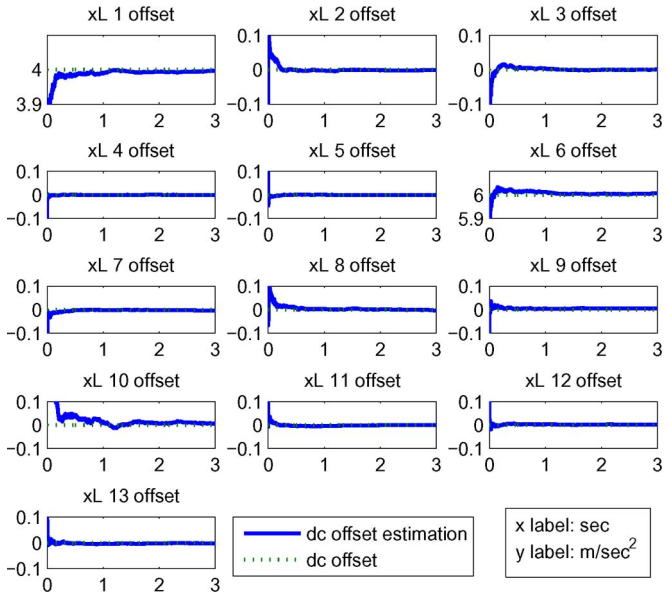

Fig. 6. Real-time dc-offset estimation for 13 accelerometer outputs. All the estimated values converge to their respective correct values. The estimation accuracy is roughly at 0.01 m/s^2.

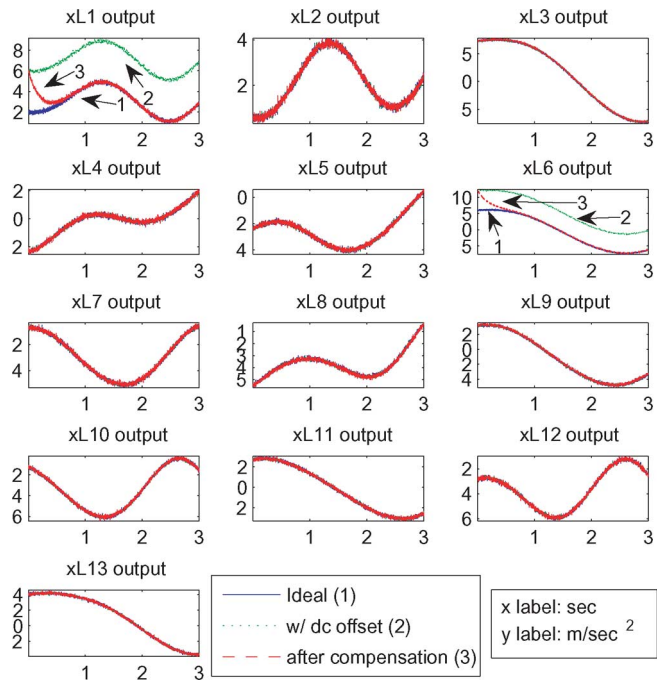

Fig. 7. Compensated accelerometer outputs converge to their respective correct values. The associated standard deviation is roughly at 0.1 m/s^2 for each compensated accelerometer output.

Fig. 9 shows the estimation of linear accelerations using the compensated accelerometer outputs. Simulation results indicate that the estimated values of linear accelerations converge to their correct values. Furthermore, the standard deviation of the estimated linear accelerations converges to 0.24 m/s^2 for F_{o1} and 0.1 m/s^2 for both F_{o2} and F_{o3}.

Fig. 10 shows the convergence of the accelerometer outputs for various feedback gains, ranging from 0.01 to 0.0035, which are used in the dc-offset compensation algorithm. To increase plot visibility, the compensated accelerometer outputs

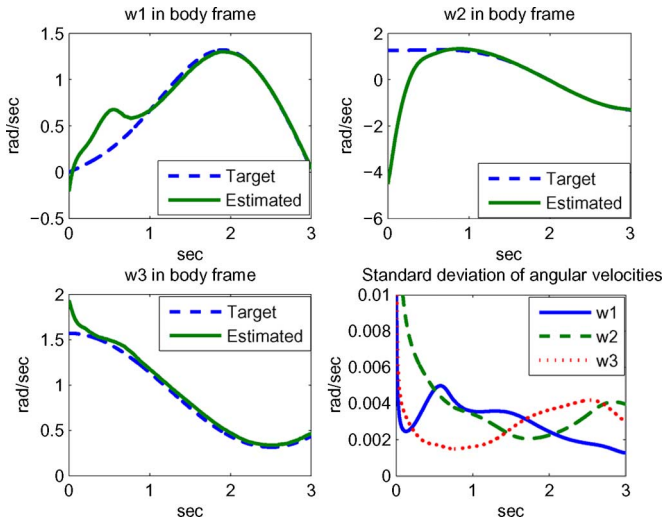

Fig. 8. Angular-velocity estimation using the compensated accelerometer outputs. Estimated values converge to the correct values (Target), respectively.

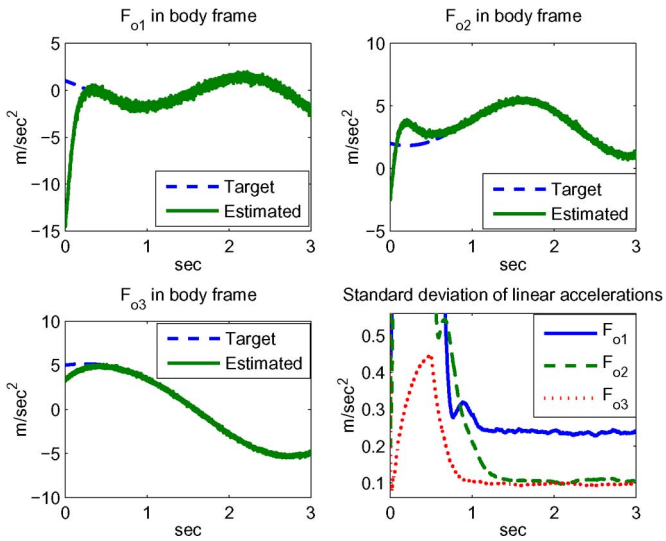

Fig. 9. Linear-acceleration estimation using the compensated accelerometer outputs. Estimated values converge to their respective correct values (Target).

are shown for xL1 and xL6 only. As evident from the plots, the convergence rate of the accelerometer outputs increases along with the feedback gain.

Fig. 11 shows the estimation of angular velocities using the compensated accelerometer outputs. The convergence of angular velocities varies depending on the feedback gain used in the compensation algorithm. The convergence time is roughly 2 s for a feedback gain of 0.01, 1.2 s for a feedback gain of 0.005, and longer than 3 s for a feedback gain of 0.0035. In this case, the convergence rate is not proportional to the feedback gain. The lower right plot shows the corresponding maximum singular values of the covariance matrix of estimated angular velocities. This covariance matrix is calculated using the IKF algorithm along with the estimation process. As shown in the plots, the singular value drops monotonically for each case.

Fig. 12 shows the case where the dc offsets of xL1 and xL6 are both 0.1 m/s^2. As evident from the plots, the proposed fault-identification method fails to detect their biased values.

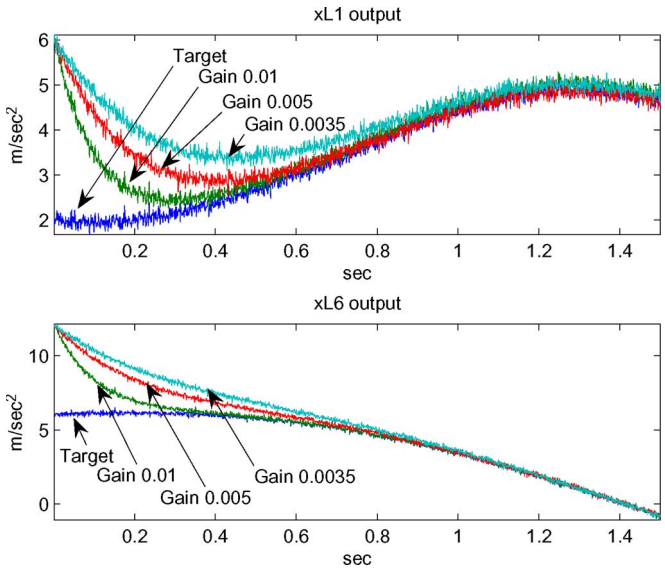

Fig. 10. Convergence of the accelerometer outputs varies depending on the feedback gain used in the compensation algorithm. The larger the feedback gain, the quicker the convergence.

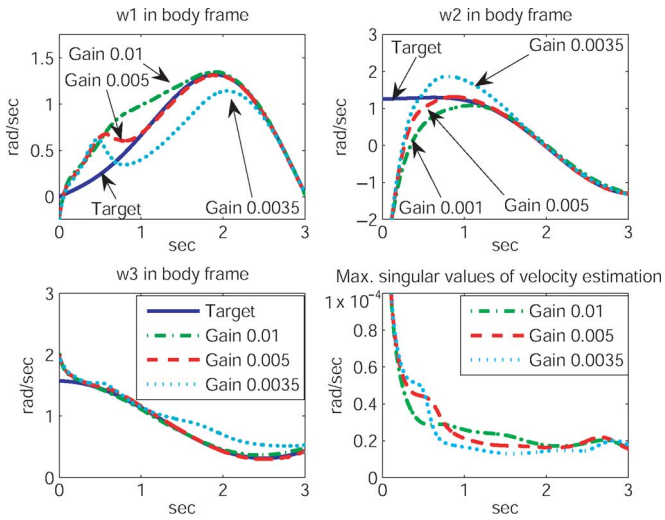

Fig. 11. Convergence of the angular velocities varies depending on the feedback gains used in the compensation algorithm. For angular velocities, a larger feedback gain does not lead to a quicker convergence.

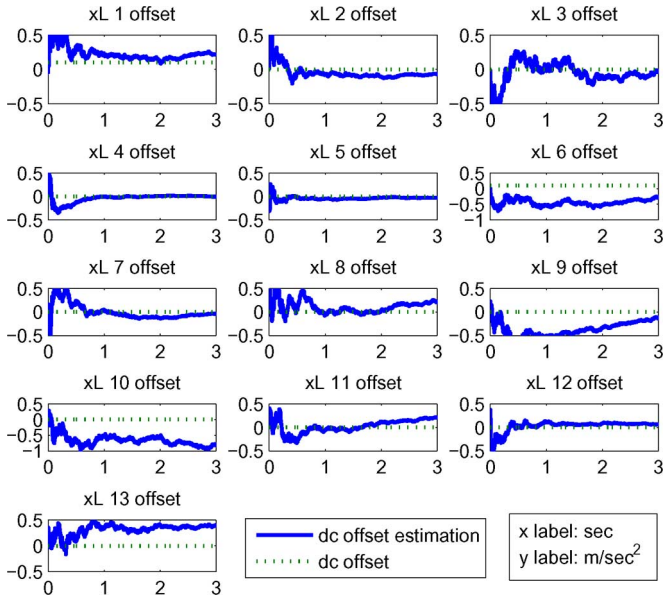

Fig. 12. Fault-identification method fails to detect the offset values for the accelerometer outputs. The offset value is 0.1 m/s^2.

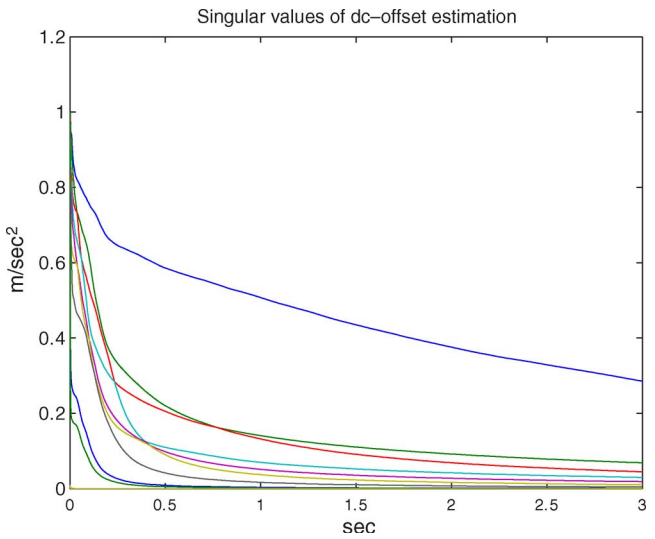

Fig. 13. Singular values of the dc-offset state covariance matrix, calculated by the associated state-estimation algorithm. The dc offset to be detected is 0.1 m/s^2. Thirteen singular values decrease monotonically with time.

However, the corresponding singular values of the state covariance matrix, which are calculated by the associated estimation algorithm (EKF), decrease monotonically, as shown in Fig. 13.

VI. Discussion

Simulation results indicate that, with the proposed compensation algorithm, the dc-offset estimation accuracy is one order less than the standard deviation of the accelerometer outputs. Therefore, the outputs of the compensated accelerometers converge to their correct values, and their standard deviations are the same as the accelerometer outputs without compensation. Consequently, the sensing resolution of a coplanar IMU that uses the compensated accelerometer outputs is the same as the one that uses no-biased accelerometer outputs. Therefore, one can conclude that the stability and the sensing resolution for the proposed coplanar gyro-free IMU system are not affected by the dc-offset compensation algorithm.

When lowering the magnitude of any dc offset that is present in the accelerometer outputs, the proposed fault-identification method fails to identify the offset value at around 0.1 m/s^2, which happens to be the standard deviation of the accelerometer measurement noise. Ideally, for a linear system, the Kalman filter algorithm can estimate states correctly for the state values less than the standard deviation of the measurement noise. In addition, the continuous decrease in singular values, as shown in Fig. 13, indicates that the employed EKF is working properly for optimal state estimation. Therefore, it could be a linearization error, which is introduced by the EKF algorithm, that

limits the detection accuracy of the proposed fault-identification design. However, more research is necessary to investigate this.

Fig. 10 shows that the convergence rate of the accelerometer output increases as the feedback gain increases. However, from experience with the LQG control method, this relation is valid only when the associated noise is relatively small. These simulation results are presented here to elucidate the fact that a quick convergence of the accelerometer outputs does not always lead to a quick convergence of the angular-velocity estimation, as shown in Fig. 11. This result could be attributed to the nonlinearity of the proposed coplanar gyro-free IMU system. Because of this, its state-convergence property depends on the state values, which are affected by the trajectory of the compensated accelerometer outputs.

VII. Conclusion

This paper presents the design procedures and the stability analysis in detail for a fault-tolerant coplanar gyro-free IMU. This design uses 13 coplanar single-axis accelerometers together with the state-estimation techniques (EKF and IKF) to perform robust six DOF measurements for an object in motion even when up to two accelerometers produce faulty outputs.

The analysis work indicates that the 13 linear accelerometers, of which eight are in-plane sensing accelerometers and five are out-of-plane sensing accelerometers, is the minimum number of accelerometers needed for this application. In the design example, these accelerometers were deployed on the periphery of a disk. Each accelerometer measurement was contaminated by noise and achieved an SNR of four for the angular-velocity estimation. The simulation results show that the proposed real-time fault-compensation algorithm can identify the faulty sensors and correct their biased values. The minimum detectable dc-offset value was equal to the standard deviation of the accelerometer measurement noise. Once the offsets were detected, the compensation accuracy became 0.01 m/s^2. Because this accuracy is one order less than the standard deviation of the accelerometer outputs, the IMU output accuracy is not affected by the compensation algorithm. Furthermore, owing to the observer-based design and the IKF techniques, the IMU system can estimate the angular velocities accurately without the need for its initial values. The estimation accuracy was 4×10^{-3} rad/s for the angular velocities and less than 0.24 m/s^2 for the linear accelerations.

Appendix
Sensing Direction of Observer Accelerometers

Let $A \in C^{m\times 6}$, where A consists of six independent column vectors and $m \geq 6$. For clarity of presentation, let $A(i,j)$ represent the component in the ith row and jth column of the A matrix; $A(:,1:3)$ represents the first three columns of the A matrix. Furthermore, let $v_i \in \text{Nullity}(A^*(:,1:3))$. Therefore

$$A^*(:,1:3)v_i = 0, \quad v_i^* A(:,1:3) = 0. \tag{25}$$

Since the rank of $A(:,1:3)$ is three, there are $m-3$ linearly independent column vectors of v_i to satisfy (25).

Let C^m denote any column vector with a dimension of m and $R(A)$ be the spans of columns of A. Therefore

$$\begin{aligned} C^m &= R\left(A(:,1:3)\right) + \text{Nullity}(A^*(:,1:3)) \\ &= R(A) + R^{\perp}(A) \\ &= R\left(A(:,1:3)\right) + R\left(A(:,4:6)\right) + R^{\perp}(A) \\ \Rightarrow \text{Nullity}&\left(A^*(:,1:3)\right) = R\left(A(:,4:6)\right) + R^{\perp}(A). \end{aligned}$$

Therefore, one can choose a minimum m of six such that the three column vectors of v_i are

$$V = \begin{bmatrix} A(:,4) + R^{\perp}\left(A(:,4:6)\right) \\ A(:,5) + R^{\perp}\left(A(:,4:6)\right) \\ A(:,6) + R^{\perp}\left(A(:,4:6)\right) \end{bmatrix}^{\mathrm{T}}$$

$$V^* A(:,4:6) = A^*(:,4:6)A(:,4:6).$$

Since $A(:,4:6)$ consists of three independent column vectors, one can easily show that the rank of $V^*A(:,4:6)$ is three.

References

[1] S. Kuo, J. Boutelle, and L. Lawdermilt, "Accelerometer input axis angular acceleration sensitivity," in *Proc. IEEE Position Location Navigat. Symp.*, San Diego, CA, Mar. 13–16, 2000, pp. 449–456.

[2] J. Randle and M. Horton, "Low cost navigation using micro-machined technology," in *Proc. IEEE ITSC*, Boston, MA, Nov. 9–12, 1997, pp. 1064–1067.

[3] J. Liu, Y. Shi, and W. Zhang, "Micro inertial measurement unit based integrated velocity strapdown testing system," *Sens. Actuators A, Phys.*, vol. 112, no. 1, pp. 44–48, Apr. 2004.

[4] Q. Wang, M. Ding, and P. Zhao, "A new scheme of non-gyro inertial measurement unit for estimating angular velocity," in *Proc. IEEE IECON*, Roanoke, VA, Nov. 2–6, 2003, vol. 2, pp. 1564–1567.

[5] W.-T. Ang, P.-K. Khosla, and C.-N. Riviere, "Design of all-accelerometer inertial measurement unit for tremor sensing in hand-held microsurgical instrument," in *Proc. IEEE Int. Conf. Robot. Autom.*, Taipei, Taiwan, R.O.C., Sep. 12–19, 2003, vol. 2, pp. 1781–1786.

[6] C. Tan, S. Park, K. Mostov, and P. Varaiya, "Design of gyroscope-free navigation systems," in *Proc. IEEE 4th Int. Conf. Intell. Transp. Syst.*, Oakland, CA, Aug. 25–29, 2001, pp. 286–291.

[7] A.-R. Schuler, A. Grammatikos, and K.-A. Fegley, "Measuring rotational motion with linear accelerometers," *IEEE Trans. Aerosp. Electron. Syst.*, vol. AES-3, no. 3, pp. 465–471, 1967.

[8] A. Selvakumar, F. Ayazi, and K. Najafi, "A high sensitivity z-axis torsional silicon accelerometer," in *IEDM Tech. Dig.*, San Francisco, CA, Dec. 8–11, 1996, pp. 765–768.

[9] H. Xie and G. K. Fedder, "A CMOS z-axis capacitive accelerometer with comb-finger sensing," in *Proc. IEEE Conf. Micro Electro Mech. Syst.*, Miyazaki, Japan, Jan. 23–27, 2000, pp. 496–501.

[10] H. Qu, D. Fang, and H. Xie, "A single-crystal silicon 3-axis CMOS-MEMS accelerometer," in *Proc. IEEE Sens. Conf.*, Vienna, Austria, Oct. 24–27, 2004, pp. 661–664.

[11] H. Kim, S. Seok, H. Kim, A. Choi, and K. Chun, "Inertial-grade out-of-plane and in-plane differential resonant silicon accelerometers (DRXLs)," in *Proc. Int. Conf. Solid-State Sens., Actuators Microsyst. (Transducers)*, Seoul, Korea, Jun. 5–9, 2005, pp. 172–175.

[12] T. Chen and S. Park, "MEMS SoC: Observer-based coplanar gyro-free inertial measurement unit," *J. Micromech. Microeng.*, vol. 15, no. 9, pp. 1664–1673, Sep. 2005.

[13] U. Krogmann, "Failure management in spatio-temporal redundant, integrated navigation and flight control reference systems," in *Proc. IEEE PLANS*, Mar. 20–23, 1990, pp. 330–337.

[14] J. Gilmore and R. McKern, "A redundant strapdown inertial reference unit (SIRC)," *J. Spacecr. Rocket*, vol. 9, no. 1, pp. 39–47, 1972.

[15] A. Ray and R. Luck, "An introduction to sensor signal validation in redundant measurement systems," *IEEE Control Syst. Mag.*, vol. 11, no. 2, pp. 44–49, Feb. 1991.

[16] K. Parsa, T. Lasky, and B. Ravani, "Design and mechatronic implementation of an accelerometer-based kinematically redundant inertial measurement unit," in *Proc. Int. Conf. Adv. Intell. Mechatronics*, Monterey, CA, Jul. 24–28, 2005, pp. 644–651.
[17] C. Chen, "Linear system theory and design," *Library of Congress Cataloging in Publication Data*, p. 367, 1984.
[18] R. Hermann and A. Krener, "Nonlinear controllability and observability," *IEEE Trans. Autom. Control*, vol. AC-22, no. 5, pp. 728–740, Oct. 1977.
[19] F. Fairman, *Linear control theory: The state space approach*. Hoboken, NJ: Wiley, 1998, pp. 147–166.
[20] M. Vidyasagar, "On the stabilization of nonlinear systems using state detection," *IEEE Trans. Autom. Control*, vol. AC-25, no. 3, pp. 504–509, Jun. 1980.
[21] Y. Bar-Shalom, X. Li, and T. Kirubarajan, *Estimation with Applications to Tracking and Navigation*. Hoboken, NJ: Wiley, 2001, p. 371.

Tsung-Lin Chen received the B.S. and M.S. degrees in power mechanical engineering from the National Tsing Hua University, Hsinchu, Taiwan, R.O.C., in 1990 and 1992, respectively, and the Ph.D. degree in mechanical engineering from the University of California, Berkeley, in 2001.

From 2001 to 2002, he was with the Analog Devices, Inc., as a MEMS Design Engineer. Since 2003, he has been with the Department of Mechanical Engineering, National Chiao Tung University, Hsinchu, where he is currently an Assistant Professor. His research interests include microelectromechanical systems and controls.